ACS APPLIED MATERIALS & INTERFACES

Research Article

www.acsami.org

Synergy between Polyaniline and OMt Clay Mineral in Langmuir–Blodgett Films for the Simultaneous Detection of Traces of Metal Ions

Anerise de Barros,[†,‡] Mariselma Ferreira,[§] Carlos José Leopoldo Constantino,[▽] José Roberto Ribeiro Bortoleto,[⊥] and Marystela Ferreira*[,‡]

[†]Faculdade de Ciências, UNESP/POSMAT, Univ Estadual Paulista, Bauru, São Paulo, Brazil

[‡]Universidade Federal de São Carlos (UFSCar), Campus Sorocaba, Sorocaba, São Paulo, Brazil

[§]Universidade Federal do ABC (UFABC), Santo André, São Paulo, Brazil

[▽]Faculdade de Ciências e Tecnologia, UNESP, Univ Estadual Paulista, Presidente Prudente, São Paulo, Brazil

[⊥]Campus Experimental de Sorocaba, Univ Estadual Paulista, Sorocaba, São Paulo, Brazil

ABSTRACT: We report on Langmuir–Blodgett (LB) films made with emeraldine salt polyaniline (PAni-ES) and organophilic montmorillonite clay mineral (OMt), where synergy between the components was reached to yield an enhanced performance in detecting trace levels of cadmium (Cd^{2+}), lead (Pb^{2+}) and copper (Cu^{2+}). Detection was carried out using square wave anodic stripping (SWAS) voltammetry with indium tin oxide (ITO) electrodes modified with LB films of PAni-ES/OMt nanocomposite, whose data were compared to those obtained with electrodes coated with neat PAni-ES and neat OMt LB films. The enhanced performance in the nanocomposite may be attributed to the stabilizing and ordering effect promoted by OMt in PAni-ES Langmuir films, which then led to more homogeneous LB films. According to X-ray diffraction data, the stacking of OMt layers was preserved in the LB films and therefore the PAni-ES chains did not cause clay mineral exfoliation. Instead, OMt affected the polaronic state of PAni-ES as indicated in UV–vis, Raman and FTIR spectra, also consistent with the changes observed for the Langmuir films. Taken together these results do indicate that semiconducting polymers and clay minerals may be combined for enhancing the electrical properties of nanostructures for sensing and related applications.

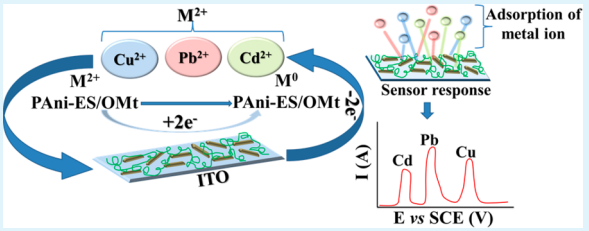

KEYWORDS: *Langmuir–Blodgett film, polyaniline, organophilic montmorilonitte clay mineral, electrochemical sensors, metal trace detection*

INTRODUCTION

Nanocomposites made with semiconducting polymer matrices[1−5] have been used in various applications, where the properties from polymers are combined with those of inorganic materials, e.g., clay mineral, for devices such as chemical sensors and biosensors.[6−11] The conducting properties of such polymers favor catalytic activity, thus increasing sensitivity, while the ability of clay minerals to exchange cations allows for detection of cationic species, including metal cations and organic molecules (e.g., water pollutants and drugs).[6−8] These nanocomposites may be fabricated in several ways,[1−5,9,12−14] with the most straightforward approach being chemical polymerization in the presence of the clay mineral. Other methods to fabricate such nanocomposites are the Langmuir–Blodgett (LB)[15−17] and self-assembly techniques,[5] including the layer-by-layer (LbL) technique.

LB films have been produced from clay minerals for various purposes, following pioneering work where organoclay complexes dispersed in a volatile organic solvent were spread at the air–water interface.[16,17] Fujimoro et al.,[18] for instance, reported on LB films where good miscibility could be achieved with a clay mineral and biodegradable polymers (e.g., poly(L-lactide), PLLA), while sensors for oxygen were fabricated with LB films containing an amphiphilic cationic iridium(III) complex and montmorillonite clay.[19] Still, with regard to sensing, Fraser et al.[20] used vermiculite clay gels with large interlayer spacing as chiral amplifiers to determine the adsorption of alanine, lysine, and histidine by chiral high-performance liquid chromatography (HPLC). Maghear et al.[21] modified glass carbon electrodes with a clay mineral to detect heavy metals such as Cu, Pb, and Cd. Detection of metal traces was possible, because of the cationic exchange with the clay minerals.

In this paper, we report on LB films made with polyaniline in the emeraldine salt form (PAni-ES) and the organophilic montmorillonite clay mineral (OMt). The interaction between PAni-ES and OMt was investigated with various methods for the

Received: January 14, 2015
Accepted: March 11, 2015
Published: March 11, 2015

DOI: 10.1021/acsami.5b00187
ACS Appl. Mater. Interfaces 2015, 7, 6828−6834

Langmuir films and LB films, while adsorption and film morphology were studied with surface plasmon resonance (SPR) and atomic force microscopy (AFM). LB films from the neat materials and the nanocomposites were used to modify electrodes to detect traces of metals that are important for environmental control.

EXPERIMENTAL SECTION

The organophilic montmorillonite clay mineral (OMt) was purchased from Cloiset Southern Clays and prepared following procedures established by Kotov et al.[16] The dispersion of OMt was obtained by sonication in a butanol−benzene mixture (1:1, v/v). The PAni-ES solution was prepared as described by Riul et al.,[22] with 1.0 mg of polyaniline emeraldine base (PAni-EB) being doped with 1.3 mg of camphorsulfonic acid (CSA) and dissolved in 1.0 mL of *m*-cresol and 9.0 mL of chloroform.

Langmuir and LB films were fabricated with a Langmuir trough (Model KSV 2000). The Langmuir films were obtained by spreading PAni-ES solution or OMt dispersion on the surface of water purified by a Millipore system (resistivity of 18.2 MΩ cm, pH adjusted to 2.5 with HCl). After spreading 50 μL of OMt dispersion, 40 min were allowed for solvent evaporation. For the PAni-ES solution, 750 μL were dispensed onto the water surface, with 15 min being allowed for solvent evaporation. To obtain the nanocomposite, OMt and PAni-ES were co-spread at the air/water interface. The surface pressure was measured with a Wilhelmy plate and film compression was performed with two movable barriers at a rate of 10.0 mm min^{-1}. The Langmuir films were transferred onto quartz, silicon, and ITO to produce Z-type LB films with three types of architecture: (i) containing only PAni-ES, (ii) only OMt, and (iii) the nanocomposite of PAni-ES/OMt. Transfer was performed at a fixed surface pressure of 30.0 to 40.0 mN m^{-1}, which is sufficiently high to ensure a condensed state, but avoiding collapse. An interval of 30 min was used between two dipping procedures, with a dipping rate of 1.5 mm min^{-1} for all cases.

The quality of LB deposition was inferred from the transfer ratio and the films were characterized by spectroscopy and microscopy analysis. For LB films deposited on quartz substrates, the ultraviolet−visible (UV-vis) spectra were taken with a Genesys Thermo Scientific Spectrometer (Model 6). FTIR and Raman spectra were obtained with LB films deposited on silicon substrates, using a Thermo Nicolet spectrometer, model Nexus 470, and a micro-Raman Renishaw spectrograph, model in-Via, equipped with a 1800 grooves/mm grating, a CCD detector, a 633-nm laser, and a Leica microscope (50× lens objective lens collecting spectra with ca. 1 μm^2 spatial resolution), with collection time of 10 s and the spectral resolution of ca. 4 cm^{-1}. X-ray diffraction (XRD) experiments were made with a Bruker diffractometer (Model D8 Discovery; Cu Kα, λ = 0.154 nm) for 20-layer LB films deposited on silicon substrates. The spectra were taken with a 0.05 step, an exposure time of 3 s, a voltage of 40 kV, and a current of 30 mA. The basal distances were calculated from the peak position using the Bragg equation. Surface plasmon resonance (SPR) measurements were performed with a SPR BioNaves model SPR Navi 200 and 670 nm laser, with films deposited onto Au plates. The surface topography of the samples was studied with atomic force microscopy (AFM) (Model XE-100, Park Systems) operating in the noncontact mode and using silicon cantilevers whose nominal radius was 5.0 nm. An area of 3.0 μm × 3.0 μm was scanned at a resolution of 522 × 512 points. From the AFM images, the surface roughness was quantified using the root-mean-square (rms) roughness.

The sensors were evaluated using a potentiostat/galvanostat (Model PGSTAT 30), coupled to the electrochemical cell, with measurements by square wave anodic stripping voltammetry (SWASV). The voltammetry analysis was made with a saturated calomel reference electrode (SCE) and a platinum counterelectrode with an area of 1.0 cm^2, an electrolytic 0.1 mol L^{-1} HCl solution with deposition potential for the species to be adsorbed of −1.0 V, an accumulation time of 300 s, an amplitude of 50 mV, and a frequency of 15 Hz. The LB films were deposited on ITO substrates for detecting Pb^{2+}, Cd^{2+} and Cu^{2+} metals ions from $PbCl_2$, $CdCl_2{\cdot}H_2O$, and $CuCl_2{\cdot}2H_2O$ salts in several concentrations. The area of the working electrode coated with LB films was 1.5 cm^2.

RESULTS AND DISCUSSION

The incorporation of OMt confers stability to the PAni-ES Langmuir film, whose collapse pressure is relatively low, as indicated in Figure 1A. Also shown is the fact that, upon

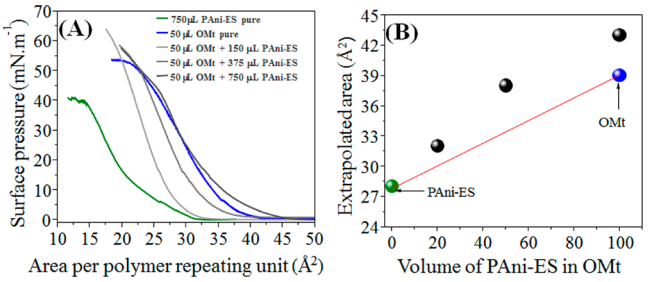

Figure 1. (A) Surface pressure isotherms for Langmuir films made with neat PAni-ES, neat OMt, and nanocomposites with distinct PAni-ES/OMt relative concentrations. (B) Extrapolated area for the various Langmuir films versus volume samples of PAni-ES mixture with OMt. This extrapolated area was obtained by prolonging the isotherm at small areas (condensed film) down to zero pressure, the value of the area being taken as the intercept with the abscissa. The solid line represents the expected dependence, should the additivity rule for immiscible components be obeyed.

increasing the relative concentration of OMt, the collapse pressure and the area per repeating unit increased, even surpassing the area measured for neat OMt. Figure 1B illustrates such behavior, which deviates strongly from the additivity rule for mixed Langmuir films. Therefore, one might infer that significant molecular-level interactions could take place between OMt and PAni-ES, perhaps with polymer chains being inserted into the OMt interlamellar spaces. However, X-ray diffraction (XRD) experiments to be reported indicate that this insertion does not occur (the OMt interlamellar structure is kept), and the changes in area may be associated with changes in the structure of the OMt layers. The stability induced by OMt was also inferred from the visual observation of stripes near the barriers for neat PAni-ES films, which were not observed in the mixed PAni-ES/OMt films. Furthermore, the composite PAni-ES/OMt film could be compressed several times, with only a small shift toward smaller areas, whereas for PAni-ES, this repeated compression−expansion procedure led to larger shifts toward lower areas per repeating unit.

Langmuir films of neat PAni-ES, OMt, and PAni-ES/OMt could be transferred onto solid substrates to form Z-type LB films, where deposition occurs only when the substrate is removed from the aqueous subphase with pH adjusted to 2.5. Film growth, as determined by measuring the UV-vis spectra shown in Figure 2, was exponential for PAni-ES, probably with preferential adsorption on sites where there is already adsorbed polymer. Figure 2A brings the spectra for 10 layers adsorbed sequentially, featuring three bands assigned to PAni at 300, 400, and 750 nm, which correspond respectively to the $\pi-\pi^*$ transition, the antiligand (π^*) transition for the polaronic band, and the polaronic state due to CSA doping.[23] The spectra for the OMt LB films are shown in Figure 2B, characterized by a band at 250 nm due to a charge transfer transition on Fe−OH groups.[24] The intensity of this band increases practically linearly, as indicated in Figure 2B. Also linear is the increase in intensity of

DOI: 10.1021/acsami.5b00187
ACS Appl. Mater. Interfaces 2015, 7, 6828−6834

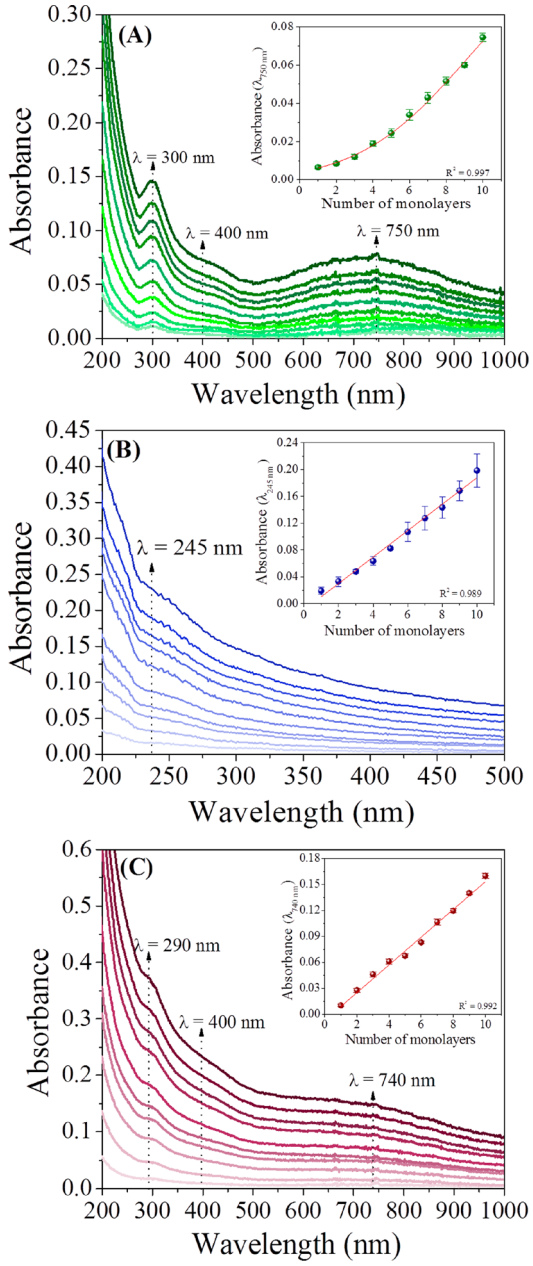

Figure 2. UV-vis spectra for LB films deposited on quartz plates with up to 10 layers of (A) PAni-ES, (B) OMt, and (C) PAni-ES/OMt. The insets depict film growth with plots of absorbance versus number of layers deposited. Absorbance was recorded at (A) 750 nm for PAni-ES, (B) 245 nm for OMt, and (C) 739 nm for PAni-ES/OMt.

the polaronic band at 739 nm for the PAni-ES/OMt LB films, whose spectra are displayed in Figure 2C. The band due to OMt is masked by the PAni-ES band at 292 nm, assigned to the $\pi-\pi^*$ transition. Note that the bands of PAni-ES in the mixed film are shifted in comparison to those in the neat LB films, consistent with molecular level interaction pointed by $\pi-A$ isotherms.

Film growth was also monitored with SPR measurements, whose data for the sequential adsorption of layers in LB films deposited onto gold are given in Figure 3. A shift in the SPR signal toward increasing angle is observed for the PAni-ES LB film in Figure 3A when the number of layers increased as the film became more optically absorptive.[25] The lowering of the SPR signal in the regions between 40° and 42° and between 48° and 50° is associated with increasing disorder in the LB film. In

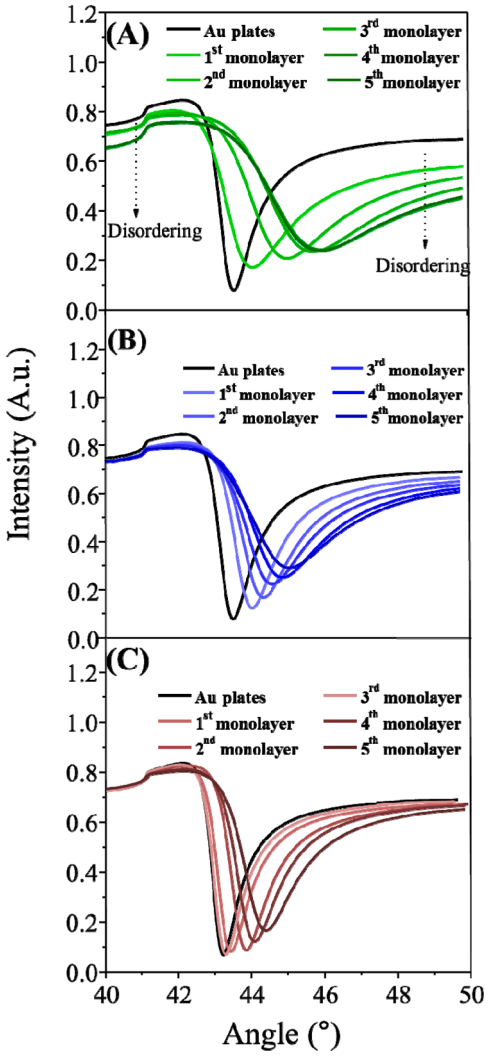

Figure 3. SPR curves with the impinging laser at 670 nm for LB films: (A) PAni-ES, (B) OMt, and (C) PAni-ES/OMt, deposited onto Au plates.

contrast, the mixed PAni-ES/OMt LB film in Figure 3C displays no sign of disordering, and there is only a shift in the angle due to increasing optical absorption as the film gets thicker. For the neat OMt LB film in Figure 3B, a shift in the angle also takes place and disordering is not very clear. In summary, the incorporation of OMt led to mixed LB films containing PAni-ES, which are better ordered than the neat PAni-ES LB films, which is consistent with the AFM images to be shown next.

The stability induced by incorporation of OMt made the LB films from the PAni-ES/OMt composite to be considerably more homogeneous than the LB films from the neat compounds, as can be seen in the AFM images in Figure 4. The root-mean-square (RMS) roughness, for instance, was 2.8 and 9.1 nm for PAni-ES and OMt clay mineral, respectively, but only 1.6 nm for the PAni-ES/OMt LB film. The largest roughness for the LB film made with OMt is due to the large aggregates that may be visualized in Figure 4B. Hence, there is a clear dispersion of the OMt clay mineral into the PAni-ES matrix in the mixed LB film.

In order to understand why PANi-ES had such strong effects on the structuring of the LB films containing OMt, we characterized the films with three other methods, namely, X-ray diffraction (XRD), Fourier transform infrared (FTIR) spectroscopy, and Raman spectroscopy. The XRD patterns in

DOI: 10.1021/acsami.5b00187
ACS Appl. Mater. Interfaces 2015, 7, 6828−6834

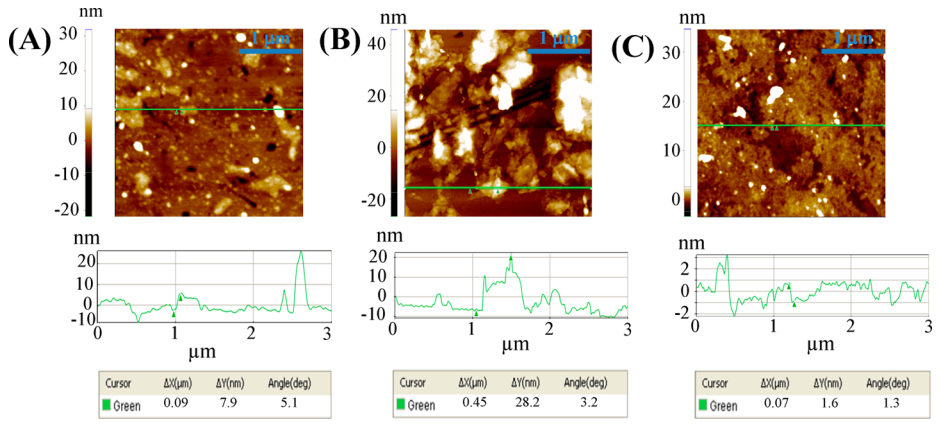

Figure 4. Atomic force microscopy (AFM) images for single-layer LB films deposited onto quartz plates: (A) PAni-ES, (B) OMt clay mineral, and (C) PAni-ES/OMt nanocomposite.

Figure 5 indicate that the stacking of the OMt layers is preserved in the mixed PAni-ES/OMt LB film. This is inferred by

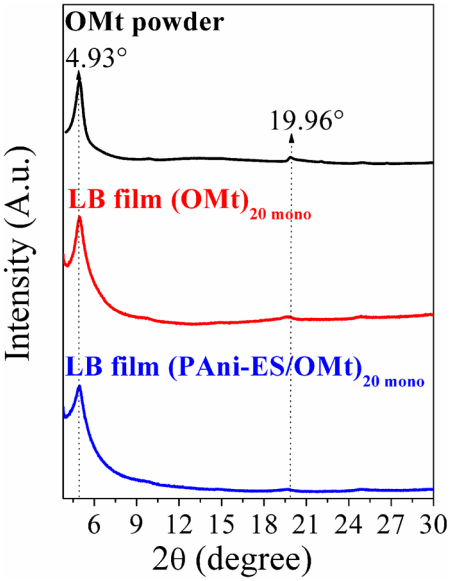

Figure 5. XRD patterns for OMt powder and 20-layer LB films of OMt and PAni-ES/OMt deposited on silicon plates.

comparing the diffractogram for OMt in powder with that of the mixed LB film. All the patterns feature peaks at 4.93° and 19.96°, with the first one corresponding to the basal spacing for the organophilic clay mineral, from which an interlamellar spacing of 1.79 nm was calculated using the Bragg equation. Therefore, the spacing is not affected when OMt is deposited in the form of LB films, either on its own or mixed with PAni-ES. The lower intensity and broadening of the 4.93° peak observed in the LB films should be ascribed to some disorder in the stacking of the clay layers. For the mixed LB film, in particular, PAni-ES chains should be outside the clay layers, just intercalating between OMt stacks.

The strong deviation from the additivity rule for the areas in the surface pressure isotherms of the mixed Langmuir films and the band shift in the UV-vis spectra of the mixed LB films appeared to point to strong molecular-level interactions, but such intimate contact between the film components is unlikely based on the XRD patterns. This apparent conflict can be resolved with FTIR and Raman spectroscopy, since molecular-level interactions should give rise to distinctive changes in the spectra for the mixed LB films in comparison to the superimposition of the spectra of the neat compounds. Figure 6 shows the FTIR spectra

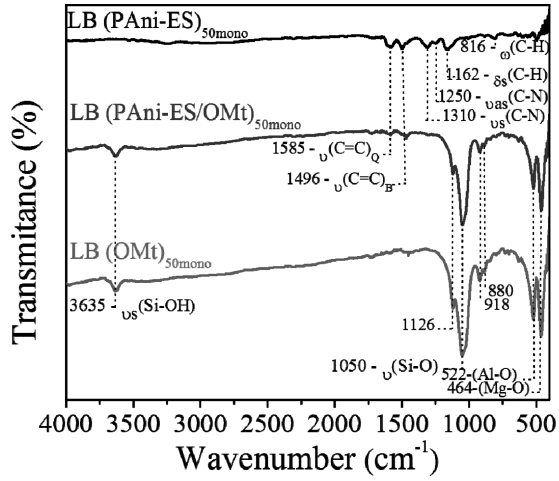

Figure 6. FTIR spectra for 50-layer LB films of PAni-ES, OMt, and PAni-ES/OMt deposited onto silicon substrates.

for 50-layer LB films of PAni-ES, OMt and mixed PAni-ES/OMt, whose main peaks are assigned in Table 1. The assignments do indicate that the transfer of PAni-ES and OMt occurred in their respective films, as their main peaks were observed. The spectrum for the PAni-ES/OMt reveals the decrease in the polaronic peaks at 1162 and 1310 cm^{-1}, assigned to N=Q=N and N−B−N modes, and at 1250 cm^{-1}, assigned to an in-plane bending vibration of Q=N^{+}H−B and B−N^{+}H−B (where Q corresponds to quinoid rings and B corresponds to benzenoid rings).[26,27] These changes are directly related to the PAni polaronic state and could be ascribed to some degree of deprotonation, since the PAni-ES chains are in contact with the OMt layers, consistent with π−A isotherms and UV-vis data.

Also consistent with the FTIR results, the Raman spectra in Figure 7 show differences between the spectrum for the PAni-ES LB film and that of the PAni-ES/OMt LB film. Peak assignment is given in Table 2. The spectrum for the OMt neat LB film is only due to the silicon substrate, as indicated in the inset. The discernible differences are again in the polaronic state at 1335 cm^{-1},[27−29] which is less pronounced in the mixed film, and the shift of the peak from 1640 cm^{-1} (PAni-ES) to 1650 cm^{-1} (PAni-

DOI: 10.1021/acsami.5b00187
ACS Appl. Mater. Interfaces 2015, 7, 6828−6834

Table 1. Assignment of FTIR Bands for LB Films of PAni-ES, OMt, and PAni-ES/OMt

PAni-ES		OMt		PAni-ES/OMt	
assignment	wavenumber (cm^{-1})	assignment	wavenumber (cm^{-1})	assignment	wavenumber (cm^{-1})
CH deflection out of plane	816	Mg−O deformation	464	Mg−O deformation	464
Vibrational Mode, N═Q═N	1162	Al−O deformation	522	Al−O deformation	522
Q=N^+H−B or B−N^+H−B stretch radical cation	1250	Al−Fe−OH bending	880	Al−Fe−OH bending	880
Vibrational Mode, N═B═N in plane	1310	Al−Al−OH stretching	918	Al−Al−OH stretching	918
		Si−O stretching	1050	Si−O stretching	1050
			1126		1126
		OH stretching	3635	OH stretching	3635
C═C stretching (benzenoid ring)	1496			C−C stretching (benzenoid)	1496
C═C stretching (quinoid ring)	1585			C−C stretching (quinoid)	1585

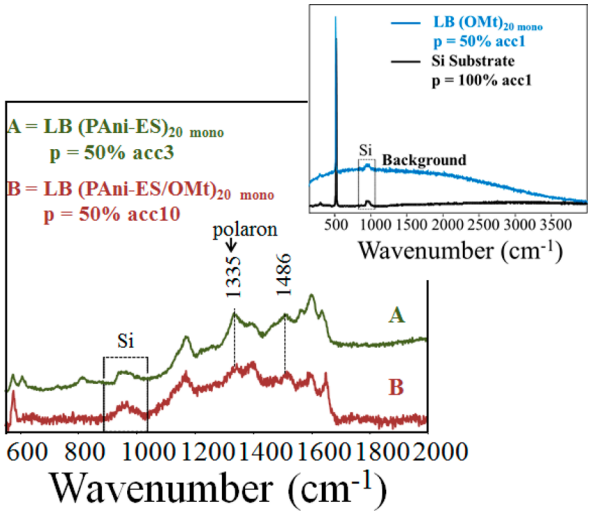

Figure 7. Raman spectra for 20-monolayer LB films onto silicon: PAni-ES (spectrum A, dark green trace) and PAni-ES/OMt (spectrum B, dark red trace). The inset corresponds to the Raman spectra of the OMt LB film and of a silicon substrate.

Table 2. Assignment of Raman Bands for LB Films of PAni-ES and PAni-ES/OMt[a]

PAni-ES		PAni-ES/OMt	
633 nm	assignment	633 nm	assignment
1640	stretching vibration of benzene ring	1650	stretching vibration of benzene ring
1600	C−C benzenoid ring stretching	1600	C−C benzenoid ring stretching
1486	C−N and CH−CH stretching vibrations	1486	C−N and CH−CH stretching vibrations
1400	C−N−C and C═N stretch	1400	C−N−C and C═N stretch
1335	cation radical (C−N^+ stretching)	1335	cation radical (C−N^+ stretching)
1180	C−H benzenoid	1180	C−H benzenoid
615	ring in plane deformation benzene radical		
580		580	ring in plane deformation benzene radical

[a]The Raman scattering spectra were recorded using λ_0 = 633 nm.

ES/OMt), because of cross-linking.[30] In summary, the incorporation of OMt tends to deprotonate some PAni-ES in mixed LB films.

Detecting Metal Ions with the LB Films. The electrochemical activity of the LB films produced can be exploited to detect metal ions using SWAS voltammetry, whose mechanism of detection is depicted in Figure 8, where the preconcentration as well as the stripping steps are shown.

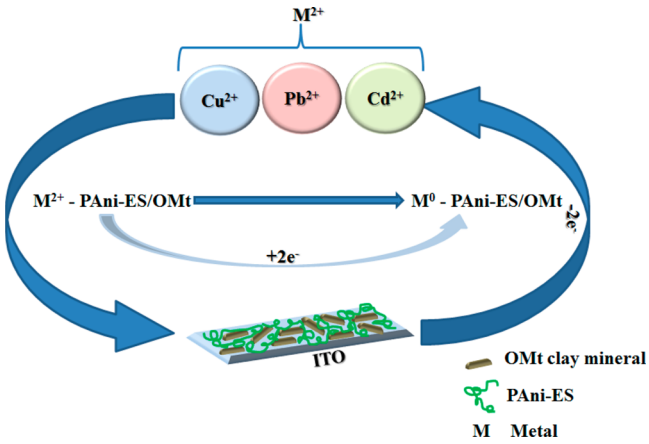

Figure 8. Mechanism behind detection of metal ions with the LB films, for the case of the PAni-ES/OMt film. The HCl electrolyte solution should contain one of the three metal ions (Cu^{2+}, Pb^{2+}, and Cd^{2+}), which would adsorb on the modified electrode (A), to be reduced (B) and then oxidized (C).

Figures 9A−C respectively show SWAS voltammograms for PAni-ES, OMt, and PAni-ES/OMt LB films deposited onto ITO electrodes in electrolyte solutions containing distinct concentrations of three metal ions. All the modified electrodes could distinguish between the three metal ions, as indicated by the oxidation peaks marked in the figures. A more clear distinction was achieved with the OMt LB film, probably because there was no interference of the oxidation peak assigned to PAni in its emeraldine salt conducting form at ca. −0.5 V for the PAni-containing electrodes. The increasing currents with the metal concentration for this peak points to chelation of the metal ions with PAni.[31] The potentials at which the peaks occurred for the three metal ions varied with the electrode used, because the ability to transfer electrons differs among the electrodes. The current of the peaks increased with the metal concentration, which allowed us to determine the sensitivity and limit of detection (LOD) from the analytical curves shown in the insets of Figures 9A−C. These values are given in Table 3.

DOI: 10.1021/acsami.5b00187
ACS Appl. Mater. Interfaces 2015, 7, 6828−6834

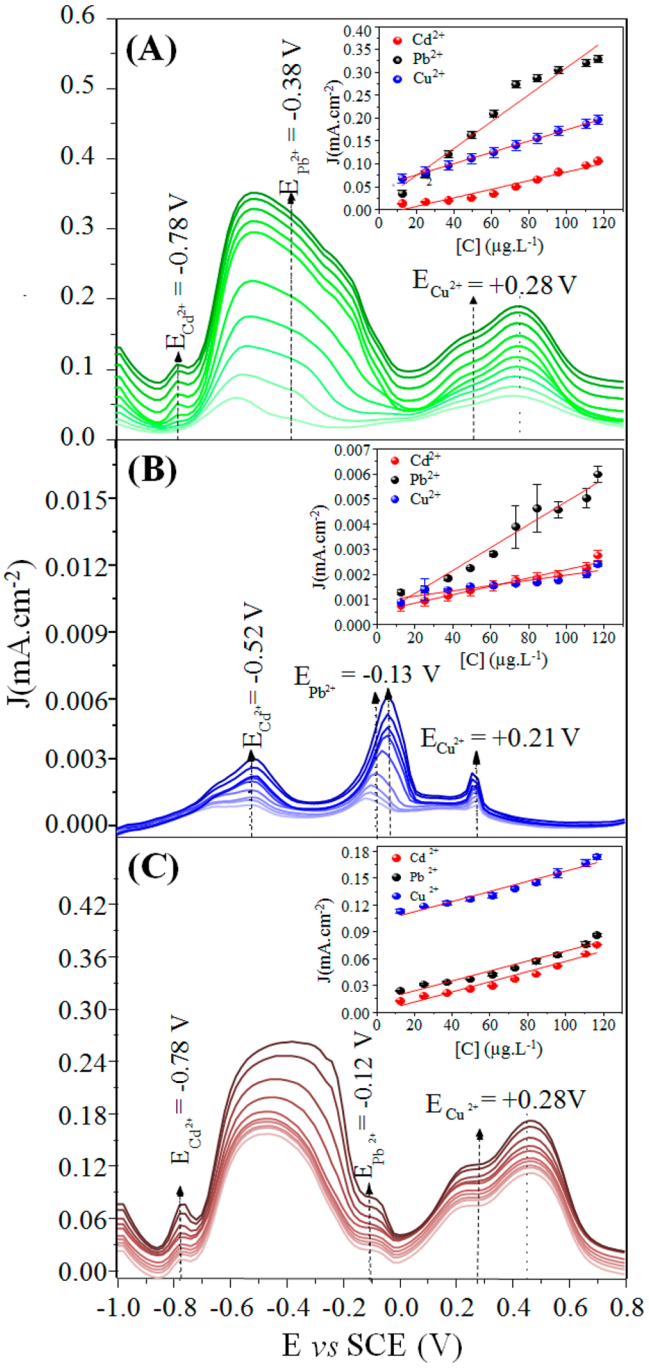

Figure 9. Square wave anodic stripping voltammograms for simultaneous detection of Cu^{2+}, Pb^{2+}, and Cd^{2+} in HCl 0.1 mol L^{-1} with a deposition potential of −1.0 V, an accumulation time of 300 s, an amplitude of 50 mV, and a frequency of 15 Hz: (A) PAni-ES LB films, (B) OMt clay LB films, and (C) PAni-ES/OMt nanocomposite LB films. All the films had 20 layers deposited onto ITO plates.

In a direct comparison of the performance of the three modified electrodes, one could have inferred that the OMt LB film was superior, judging by the data in Table 3. However, the peaks for this electrode in Figure 9B appear at E = −0.52, −0.13, and +0.21 V for Cd^{2+}, Pb^{2+}, and Cu^{2+}, respectively, which are shifted considerably from the expected potentials from the literature, which should be $E°$ = −0.75 V for Cd^{2+}, $E°$ = −0.51 V for Pb^{2+}, and $E°$ = +0.34 V for Cu^{2+}.[32] Furthermore, in subsidiary experiments, we noted that the reproducibility of the electrochemical measurements under the same conditions for the OMt LB film was not as good as for the PAni-ES/OMt and PAni-ES LB films. We conclude that the electrode coated with the nanocomposite, i.e. PAni-ES/OMt, is the most efficient in detecting the three metal ions simultaneously because separation is more efficient than for the PAni-ES LB film, which can be seen by comparing Figure 9C with Figure 9A. There is no overlap for the PAni-ES/OMt LB film with the peaks at −0.5 V and +0.45 V, characteristic of PAni-ES, while the shift in the Pb^{2+} and Cu^{2+} peak is ascribed to chelate formation when the ions are adsorbed on the electrode surface. In summary, this superior performance for the PAni-ES/OMt LB film points to synergy between the materials in this sensing task. The results can be compared to similar response obtained with the materials immobilized by the LbL technique reported by de Barros et al.[33]

Table 3. Adsorbed Amounts on Modified Surfaces of PAni-ES, OMt, and PAni-ES/OMt LB Films[a]

analyte (metal traces)	electrode modified	potential (V)	sensitivity (μA μg L^{-1})	LOD (μg L^{-1})
Cd^{2+}	PAni-ES	−1.0	0.9470 ± 0.0775	0.2455
Pb^{2+}	PAni-ES	−1.0	2.9392 ± 0.2183	0.2228
Cu^{2+}	PAni-ES	−1.0	1.2326 ± 0.0151	0.0367
Cd^{2+}	OMt	−1.0	16.6708 ± 1.1854	0.2133
Pb^{2+}	OMt	−1.0	10.4739 ± 1.4789	0.4236
Cu^{2+}	OMt	−1.0	45.8811 ± 3.1060	0.2031
Cd^{2+}	PAni-ES/OMt	−1.0	0.5632 ± 0.0494	0.2631
Pb^{2+}	PAni-ES/OMt	−1.0	0.5607 ± 0.0434	0.2324
Cu^{2+}	PAni-ES/OMt	−1.0	0.5716 ± 0.0402	0.2113

[a]The sensitivity of the neat OMt sensing unit is higher, but its LOD is not lower than for the PAni-ES/OMt LB film, because its reproducibility is worse, which leads to larger dispersion in the data.

CONCLUSION

The Langmuir−Blodgett (LB) technique has been proven suitable to fabricate nanocomposites containing polyaniline and OMt clay, where the latter imparted stability to PAni-ES Langmuir films with which homogeneous LB films could be obtained. The additivity rule was not obeyed for the mixed PAni-ES/OMt Langmuir films, suggestion molecular-level interactions leading to changes in the PAni-ES conformation chains, which may be enveloping OMt layers. The X-ray diffraction data showed preserved stacking of the OMt layers in the mixed PAni-ES/OMt LB film. The molecular-level interactions was confirmed with FTIR and Raman spectroscopies, with incorporation of OMt affecting the polaronic state of the PAni-ES chains, consistent with UV-vis data.

The combination of OMt and PAni-ES was such that improved electrochemical properties could achieve in the PAni-ES/OMt LB films, which then allowed modified ITO electrodes to be used in detecting metal ions. Using SWAS voltammetry, simultaneous detection of three metal ions was made possible, with the lowest limit of detection being reached for the electrode modified with PAni-ES/OMt LB films, thus confirming the synergy between the two materials.

DOI: 10.1021/acsami.5b00187
ACS Appl. Mater. Interfaces 2015, 7, 6828−6834

AUTHOR INFORMATION

Corresponding Author

*Tel.: +55 15 3229 5969. Fax: +55 15 3229 6000. E-mail: marystela@ufscar.br.

Notes

The authors declare no competing financial interest.

ACKNOWLEDGMENTS

The authors are grateful to FAPESP (Nos. 2011/00733-2 and 2012/16158-0), CNPq (No. 473222/2012-4), CAPES, and nBioNet network for the financial support. The authors also acknowledge Prof. Osvaldo N. Oliveira, Jr., for helpful discussions, and Dr. Priscila A. Constantino, for help with the Raman measurements.

REFERENCES

(1) Bitinis, N.; Hernandez, M.; Verdejo, R.; Kenny, J. M.; Lopez-Manchado, M. A. Recent Advances in Clay/Polymer Nanocomposites. *Adv. Mater.* **2011**, *23*, 5229−5236.

(2) Chiu, C.-W.; Lin, J.-J. Self-Assembly Behavior of Polymer-Assisted Clays. *Prog. Polym. Sci.* **2012**, *37*, 406−444.

(3) Kehlbeck, J. D.; Hagerman, M. E.; Cohen, B. D.; Eliseo, J.; Fox, M.; Hoek, W.; Karlin, D.; Leibner, E.; Nagle, E.; Nolan, M.; et al. Directed Self-Assembly in Laponite/CdSe/Polyaniline Nanocomposites. *Langmuir* **2008**, *24*, 9727−9738.

(4) Baldissera, A. F.; Souza, J. F.; Ferreira, C. A. Synthesis of Polyaniline/clay Conducting Nanocomposites. *Synth. Met.* **2013**, *183*, 69−72.

(5) Chiu, C.-W.; Huang, T.-K.; Wang, Y.-C.; Alamani, B. G.; Lin, J.-J. Intercalation Strategies in Clay/polymer Hybrids. *Prog. Polym. Sci.* **2014**, *39*, 443−485.

(6) Luo, L.; Wang, X.; Ding, Y.; Li, Q.; Jia, J.; Deng, D. Voltammetric Determination of Pb^{2+} and Cd^{2+} with Montmorillonite-Bismuth-Carbon Electrodes. *Appl. Clay Sci.* **2010**, *50*, 154−157.

(7) Mousty, C. Sensors and Biosensors Based on Clay-Modified Electrodes? New Trends. *Appl. Clay Sci.* **2004**, *27*, 159−177.

(8) Junxiang, H.; Sato, H.; Umemura, Y.; Yamagishi, A. Sensing of Molecular Chirality on an Electrode Modified with a Clay−Metal Complex Hybrid Film. *J. Phys. Chem. B* **2005**, *109*, 4679−4683.

(9) Rajapakse, R. M. G.; Murakami, K.; Bandara, H. M. N.; Rajapakse, R. M. M. Y.; Velauthamurti, K.; Wijeratne, S. Preparation and Characterization of Electronically Conducting Polypyrrole-Montmorillonite Nanocomposite and Its Potential Application as a Cathode Material for Oxygen Reduction. *Electrochim. Acta* **2010**, *55*, 2490−2497.

(10) Sierra, I.; Hierro, I.; Pérez-Quintanilla, D.; Morante-Zancero, S.; Sánchez, A. Development of Screen-Printed Carbon Electrodes Modified with Functionalized Mesoporous Silica Nanoparticles: Application to Voltammetric Stripping Determination of Pb(II) in Non-Preteated Natural Waters. *Electrochim. Acta* **2010**, 6983−6990.

(11) Armstrong, K. C.; Tatum, C. E.; Dansby-Sparks, R. N.; Chambers, J. Q.; Xue, Z. L. Individual and Simultaneous Determination of Lead, Cadmium, and Zinc by Anodic Stripping Voltammetry at a Bismuth Bulk Electrode. *Talanta* **2010**, *82*, 675−680.

(12) Haldar, I.; Biswas, M.; Nayak, A.; Ray, S. S. Dielectric Properties of Polyaniline−Montmorillonite Clay Hybrids. *J. Nanosci. Nanotechnol.* **2013**, *13*, 1824−1829.

(13) Cheng, H.-Y.; Weng, C.-J.; Liou, S.-J.; Yeh, J.-M.; Liu, S.-P. Studies on Heterogeneous Nucleation Effect of Dispersing Intercalated Montmorillonite Clay Platelets in Polyaniline Matrix. *Polym. Compos.* **2010**, *31*, 2049−2056.

(14) Bober, P.; Stejskal, J.; Špírková, M.; Trchová, M.; Varga, M.; Prokeš, J. Conducting Polyaniline−montmorillonite Composites. *Synth. Met.* **2010**, *160*, 2596−2604.

(15) Ras, R. H. A.; Umemura, Y.; Johnston, C. T.; Yamagishi, A.; Schoonheydt, R. A. Ultrathin Hybrid Films of Clay Minerals. *Phys. Chem. Chem. Phys.* **2007**, *9*, 918.

(16) Kotov, N. A.; Meldrum, F. C.; Fendler, J. H.; Tombacz, E.; Dekany, I. Spreading of Clay Organocomplexes on Aqueous Solutions: Construction of Langmuir−Blodgett Clay Organocomplex Multilayer Films. *Langmuir* **1994**, *10*, 3797−3804.

(17) Inukai, K.; Hotta, Y.; Taniguchi, M.; Tomura, S.; Yamagishi, A. Formation of a Clay Monolayer at an Air−water Interface. *J. Chem. Soc. Chem. Commun.* **1994**, 959−959.

(18) Fujimori, A.; Arai, S.; Kusaka, J.; Kubota, M.; Kurosaka, K. Formation and Structure of Langmuir−Blodgett Films of Organo-Modified Aluminosilicate with High Surface Coverage. *J. Colloid Interface Sci.* **2013**, *392*, 256−265.

(19) Morimoto, K.; Nakae, T.; Ohara, K.; Tamura, K.; Nagaoka, S.; Sato, H. Dual Emitting Langmuir−Blodgett Films of Cationic Iridium Complexes and Montmorillonite Clay for Oxygen Sensing. *New J. Chem.* **2012**, *36*, 2467.

(20) Fraser, D. G.; Fitz, D.; Jakschitz, T.; Rode, B. M. Selective Adsorption and Chiral Amplification of Amino Acids in Vermiculite Clay—Implications for the Origin of Biochirality. *Phys. Chem. Chem. Phys.* **2011**, *13*, 831−838.

(21) Maghear, A.; Tertiş, M.; Fritea, L.; Marian, I. O.; Indrea, E.; Walcarius, A.; Săndulescu, R. Tetrabutylammonium-Modified Clay Film Electrodes: Characterization and Application to the Detection of Metal Ions. *Talanta* **2014**, *125*, 36−44.

(22) Riul, A., Jr; Mattoso, L. H. C.; Telles, G. D.; Herrmann, P. S. P.; Colnage, L. A.; Parizotto, N. A.; Baranauskas, V.; Faria, R. M.; Oliveira, O. N., Jr. Characterization of Langmuir−Blodgett Films of Parent Polyaniline. *Thin Solid Films* **1996**, *284*, 177−180.

(23) Ram, M. K.; Salerno, M.; Adami, M.; Faraci, P.; Nicolini, C. Physical Properties of Polyaniline Films: Assembled by the Layer-by-Layer Technique. *Langmuir* **1999**, *15*, 1252−1259.

(24) Karickhoff, S. W.; Bailey, G. W. Optical Absorption Spectra of Clay Minerals. *Clays Clay Min.* **1973**, *21*, 59−70.

(25) Ekgasit, S.; Tangcharoenbumrungsuk, A.; Yu, F.; Baba, A.; Knoll, W. Resonance Shifts in SPR Curves of Nonabsorbing, Weakly Absorbing, and Strongly Absorbing Dielectrics. *Sens. Actuators B* **2005**, *105*, 532−541.

(26) Thomas, P.; Dwarakanath, K.; Varma, K. B. R. In Situ Synthesis and Characterization of polyaniline−$CaCu_3Ti_4O_{12}$ Nanocrystal Composites. *Synth. Met.* **2009**, *159*, 2128−2134.

(27) Ferreira, M.; Wohnrath, K.; Torresi, R. M.; Constantino; Aroca, R. F.; Oliveira; Giacometti, J. A. Spectroscopic and Electrochemical Characterization of Polyaniline and a Ruthenium Complex, Mer-$[RuCl_3(dppb)(py)]$, in the Form of Langmuir−Blodgett Films. *Langmuir* **2002**, *18*, 540−546.

(28) Do Nascimento, G. M.; Constantino, V. R. L.; Landers, R.; Temperini, M. L. A. Spectroscopic Characterization of Polyaniline Formed in the Presence of Montmorillonite Clay. *Polymer* **2006**, *47*, 6131−6139.

(29) Do Nascimento, G. M.; Temperini, M. L. A. Structure of Polyaniline Formed in Different Inorganic Porous Materials: A Spectroscopic Study. *Eur. Polym. J.* **2008**, *44*, 3501−3511.

(30) Šeděnková, I.; Trchová, M.; Stejskal, J. Thermal Degradation of Polyaniline Films Prepared in Solutions of Strong and Weak Acids and in Water—FTIR and Raman Spectroscopic Studies. *Polym. Degrad. Stab.* **2008**, *93*, 2147−2157.

(31) Li, X.; Wang, Y.; Yang, X.; Chen, J.; Fu, H.; Cheng, T.; Wang, Y. Conducting Polymers in Environmental Analysis. *TrAC, Trends Anal. Chem.* **2012**, *39*, 163−179.

(32) Silva, P.; El Khakani, M.; Chaker, M.; Dufresne, A.; Courchesne, F. Simultaneous Determination of Cd, Pb, and Cu Metal Trace Concentrations in Water Certified Samples and Soil Extracts by Means of Hg-Electroplated-Ir Microelectrode Array Based Sensors. *Sens. Actuators B* **2001**, *76*, 250−257.

(33) De Barros, A.; Ferreira, M.; Constantino, C. J. L.; Ferreira, M. Nanocomposites Based on LbL Films of Polyaniline and Sodium Montmorillonite Clay. *Synth. Met.* **2014**, *197*, 119−125.

DOI: 10.1021/acsami.5b00187
ACS Appl. Mater. Interfaces 2015, 7, 6828−6834